JOURNAL OF MATERIALS SCIENCE: MATERIALS IN MEDICINE **16** (2005) 229–237

Laser bonded microjoints between titanium and polyimide for applications in medical implants

A. MIAN[1], G. NEWAZ[1,2,3,*], L. VENDRA[1], N. RAHMAN[1], D. G. GEORGIEV[2], G. AUNER[2], R. WITTE[4], H. HERFURTH[4]
[1]*Department of Mechanical Engineering,* [2]*Center for Smart Sensors and Integrated Microsystems (SSIM), and* [3]*Institute for Manufacturing Research, Wayne State University, Detroit, Michigan, USA*
E-mail: gnewaz@eng.wayne.edu
[4]*Center for Laser Technology, Fraunhofer USA, Plymouth, Michigan, USA*

Bioencapsulation of medical implant devices, and neural implant devices in particular, requires development of reliable hermetic joints between packaging materials that are often dissimilar. Titanium-polyimide is one of the biocompatible material systems, which are of interest to our research groups at Wayne State University and Fraunhofer USA. We have found processing conditions for successful joining of titanium with polyimide using near-infrared diode lasers or fiber lasers along transmission bonding lines with widths ranging from 200 to 300 μm. Laser powers of 2.2 and 3.8 W were used to create these joints. Laser-joined samples were tested in a microtester under tensile loading to determine joint strengths. In addition, finite element analysis (FEA) was conducted to understand the stress distribution within the bond area under tensile loading. The FEA model provides a full-field stress distribution in and around the joint that cause eventual failure. Results from the investigation provide an initial approach to characterize laser-fabricated microjoints between dissimilar materials that can be potentially used in optimization of bio-encapsulation design.

1. Introduction

Physiological functions that are destroyed or impaired either by disease or accidents can, in principle, be restored by using active biomedical implants. Advanced micro-technologies offer new opportunities for the development of these active implants. Currently, the implants such as pacemakers [1] and cochlea implants [2, 3] are being used to treat cardiac and hearing disorders, respectively. Examples of other implants include neural and muscular stimulators for the treatment of seizures caused by epilepsy [4, 5], and implantable drug delivery systems to locally effuse chemicals and drugs such as pain medication, hormones and other pharmaceutical compounds [6–8]. Research is underway to develop subretinal implant devices that will replace damaged photoreceptor cells [9, 10]. These damaged cells fail to send electrical signals to the rest of the eye and eventual the brain, that results in blindness. The study of Humayun *et al*. [11] has showed successful results to restore vision by permanently implanting a retinal prosthesis in the blind eye. These active implants utilize microelectronic devices that are developed on biologically toxic materials such as silicon. Thus, the implantation devices need to be packaged to have a biocompatible tissue interface and to withstand biodegradation in the body. Established biocompatible materials such as titanium, glass and specific ceramics are currently being used for electronics housing in pacemakers. Flexible structures like electrode wires and lead-outs are insulated and covered with silicone rubber (PMS = Poly (Dimethyl Siloxane)), polyurethane and other polymer materials which have been extensively tested for their biocompatibility [12].

The need to join dissimilar materials occurs as the encapsulation includes functional elements such as electrodes used for neural stimulation or modules with defined micro-pores for the effusion of drugs. Proven methods for adhesive-free localized joining and hermetic sealing of non-metals and dissimilar material combinations in particular, do not yet exist for implantable microsystems. Today, adhesives and soldering are widely used to join dissimilar materials, however there are many drawbacks. Lack of long-term stability and biocompatibility are critical factors that limit their application for microsystems used in the

*Author to whom all correspondence should be addressed.

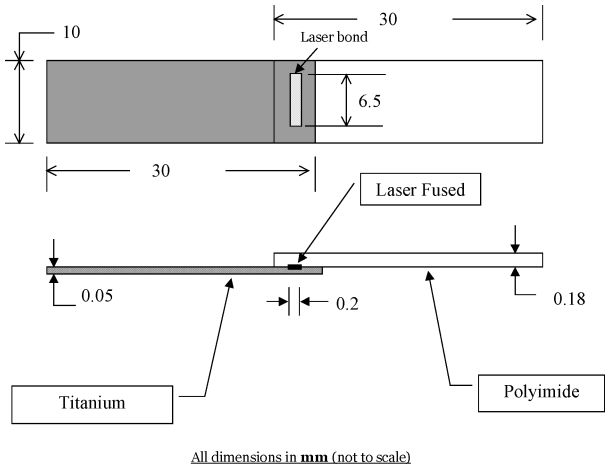

Figure 1 Sample dimensions.

biomedical sector. In addition, high heat input of soldering and the material shrinkage during curing of adhesives makes precision alignment difficult and automation very challenging. The laser micromachining procedure can overcome these limitations with its excellent focusibility to spot sizes in the micrometer range. In addition, precise control of the laser energy in the focal spot enables a very localized materials processing with minimum heat affect on the overall part.

Biocompatible materials such as titanium and polyimide are potential candidates in encapsulating implant devices. In this study, the titanium foil and polyimide sheet were joined using a transmission type laser-joining procedure. The bi-material systems was subjected to tensile loading using a microtester, and failure loads per unit bond length were documented. The failed samples were then inspected under an optical microscope, and micrographs of the surfaces near the bond areas were analyzed. In addition, Ti/polyimide interfaces obtained by laser joining were studied by X-ray photoelectron spectroscopy (XPS) in order to clarify the chemistry of the joint formation. The tensile test procedure was also simulated by employing finite element analysis (FEA) technique to numerically understand the stress distribution in the bond area. From the FEA model, failure load along with the location of failure initiation is predicted and compared with the experimental results.

2. Sample preparation and fabrication

A 4-axis high precision laser motion system that manipulates the samples under the stationary beam was used to prepare the samples. This system provides a positioning accuracy of ± 1 μm. It is well suited for testing bonding feasibility and can also provide the required precision to process small features of device structures developed within the scope of this program. Three different laser sources with micro-machining capabilities are connected to this motion system using a fiber optical beam delivery. They are 30 W continuous wave (cw) diode laser, wavelength 808 nm, minimum spot size 800 μm; 1 kW cw Nd:YAG laser, wavelength 1064 nm, minimum spot size 150 μm; and 25 W cw fiber laser, wavelength 1064 nm, minimum spot size 9 μm. For the current study, titanium/polyimide samples were fabricated using the 30 W cw diode laser that can generate a spot of minimum 800 μm. Two types of polyimide/titanium foil samples were studied in this work: samples prepared using laser power of 2.2 W and feed of 100 mm/min are labeled TYPE 1, and those made at laser power of 3.8 W and a feed rate of 1300 mm/min are labeled as TYPE 2 samples. A schematic of sample geometry and size is given in Fig. 1. The polyimide sheets were made of thermoplastic polyimide Imidex (Wastelake Plastic Company) and the titanium foil was of 99.6% purity (Goodfellow Corporation). The surfaces of titanium and polyimide were cleaned with acetone prior to placing them in the laser bonder. No additional surface treatment was performed on titanium.

The applicability of laser joining for a specific material combination and the selection of the appropriate approach depends on the optical properties of the materials. Based on the optical properties, the appropriate laser wavelength is selected to pursue either bonding or welding. A preferred approach for materials with different optical properties is transmission joining [13, 14] in an overlap configuration (Fig. 2). In this case, both materials are clamped on top of each other and the joint is created directly at the interface between the two parts based on the localized heat input of the laser. This is achieved by selecting a laser wavelength that can penetrate the top material and then is absorbed at the surface of the bottom material. Transmission joining is successfully applied in

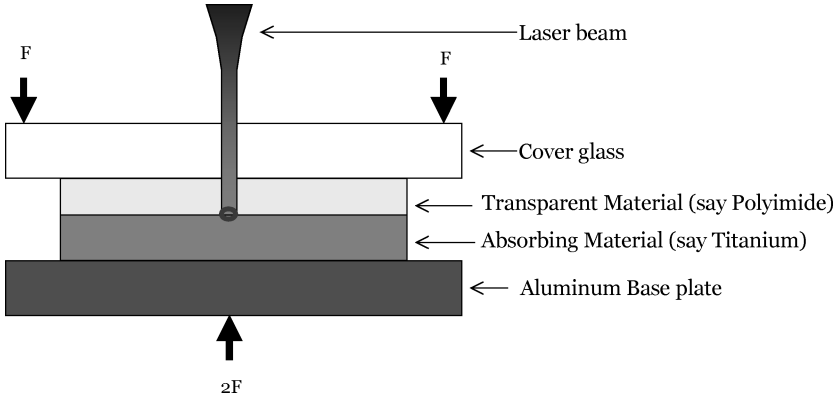

Figure 2 Transmission joining of two materials using a laser beam.

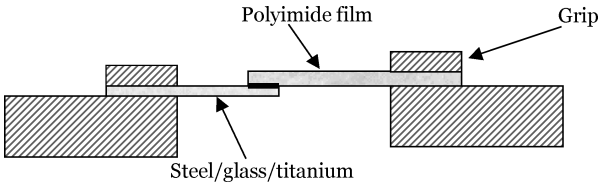

Figure 3 Schematic of a sample in the test fixture.

industry for plastic welding [15–17] and offers great potential for joining of dissimilar material combinations such as glass-to-silicon [13, 18] and polymer-to-metal [14, 18].

3. Experimental methods for sample characterization

The samples were experimentally characterized by mechanical tensile testing, optical microscopy and XPS. A brief description of the characterization procedure is given below.

3.1. Mechanical tensile tests

The samples were gripped in a microtester as shown in Fig. 3 for bond strength measurements. Details of the tensile tester are given in Fig. 4. The testing machine was a 6-axis sub-micron tester [14, 19], which is a general-purpose micromechanical/thermal testing instrument, fully controlled by a PC computer. It allows the application of displacements/loads to the tested specimen along six degrees of freedom, i.e., three orthogonal translations and three rotations. The displacement resolution of each closed-loop, DC-motor-drive stage is maintained at 0.1 mm in translations and 0.001 degree in rotations. A capacitance gage or a linear encoder is used to measure the actual displacement of a test sample. To maintain the proper alignment as shown in Fig. 3, the left and right grips of the tester were first brought close to each other (Fig. 5). A titanium test foil was kept on the top surface of the left grip, and a level gage was placed as shown in Fig. 5. The y-axis movement of the right grip was adjusted manually using the microcontroller so that the left grip (along with the titanium foil) and the right grip are at the same level.

3.2. Microscopy

The failed samples were studied by optical microscopy to study the failure surfaces in the bond areas on both the substrates (e.g. titanium and polyimide) using Olympus model BX 60 optical microscope with a magnification of 200×. The microstructure was investigated carefully and the images are discussed later.

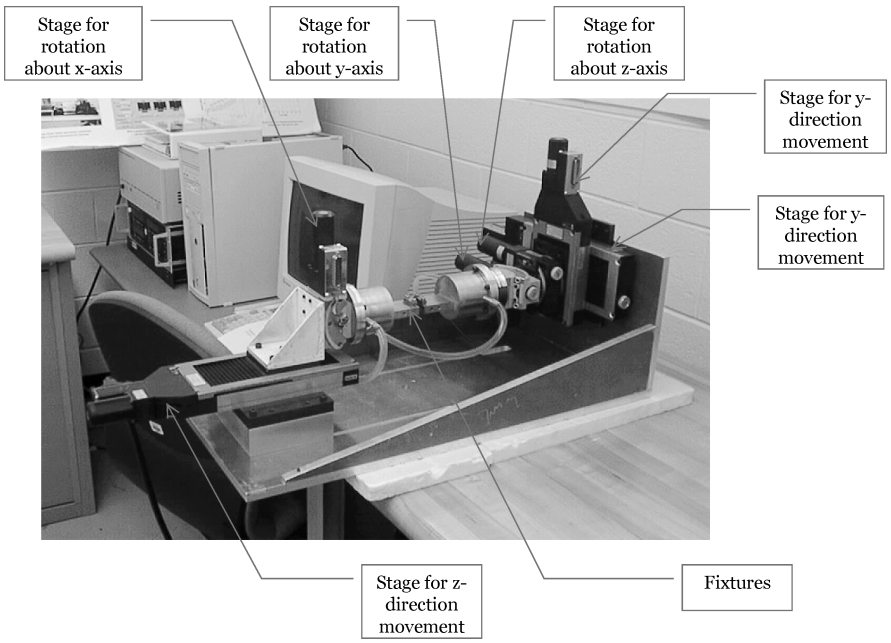

Figure 4 6-axis microtester for tensile/fatigue tests.

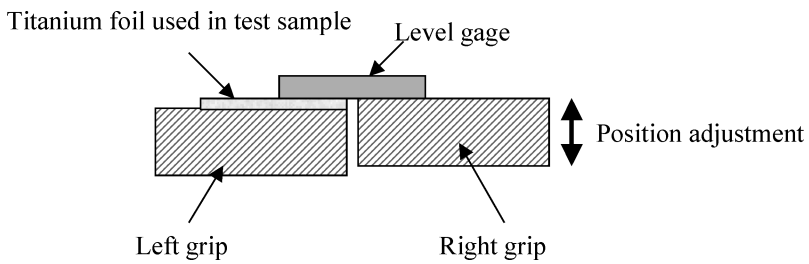

Figure 5 Adjustment of the grip to ensure symmetrical load at the bondline.

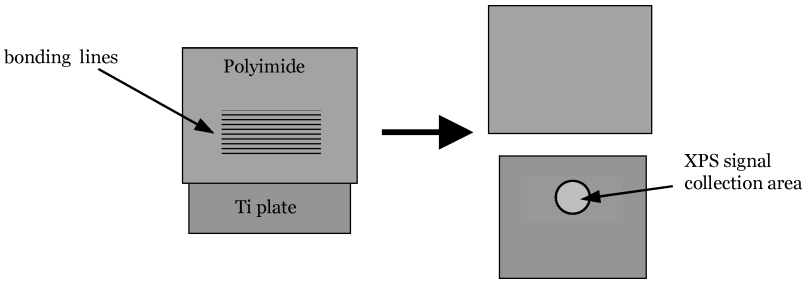

Figure 6 Sample configuration for XPS test setup.

3.3. Spectroscopy

As part of a separate study, samples consisting of polyimide bonded to a Ti plate through several parallel joint lines were prepared using similar laser parameters as was used for type 1 samples. Sample configuration for this part of the test is shown in Fig. 6. The sample was split (peeled off) into its polyimide and Ti counterparts and immediately introduced into the ultra-high vacuum chamber of a XPS spectrometer (Perkin Elmer, model 5500). The sample was studied at a vacuum of 5×10^{-10} Torr. Aluminum X-rays were used to excite the spectra and Ar-ion beam sputtering was employed to obtain XPS spectra as a function of depth from the failure surface level.

4. Finite element analysis

The commercially available FEA package ABAQUS [20] was used to develop a finite element model to better understand the stress distribution within the joining area while the bi-material system was loaded with tension. The joint was assumed to be a two dimensional plane-strain problem, such that only its longitudinal cross-section needed to be modeled. The zoomed-in mesh density and applied boundary and loading conditions are shown in Fig. 7. Geometry of the model in Fig. 7 represents true dimensions of the sample that was used for experiments and is given in Fig. 1. The point where the edge of polyimide is bonded with titanium is designated as A, and the point where the edge of titanium is bonded to polyimide is designated as B. Thus, the bondline between titanium and polyimide in this case is AB. In the model, the bondline AB was considered to be strong, and was modeled by using a common set of nodes at the titanium-polyimide interface. The common interfacial nodes are shared by elements corresponding to both titanium and polyimide. Effect of thickness of the very thin chemical bond created between titanium and polyimide was neglected. The applied boundary conditions were such that titanium end of the joint was clamped, i.e. no movements in either the horizontal (x) or vertical (y) direction were allowed. The other (polyimide) end was restrained in the horizontal (x) direction, whereas its vertical (y-direction) nodal deflections were prescribed to be equal. A displacement of 1.0 mm was applied at the polyimide end with 20 incremental steps, and static analysis was performed. Load at every incremental step was calculated by summing up the reaction forces at the fixed end. The reaction force per unit bond length was plotted against the incremental displacement load, was compared with the experimental load displacement plot.

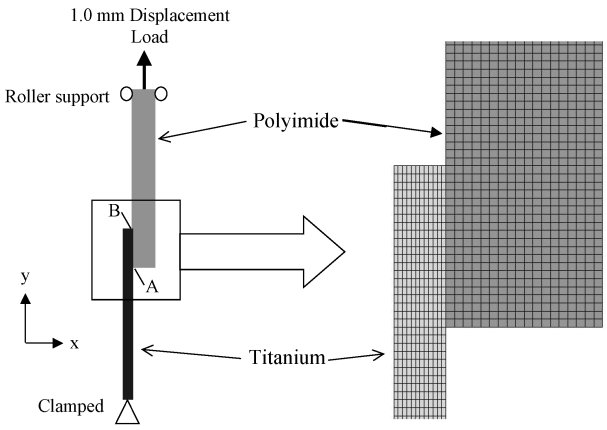

(a) Boundary and loading condition (not to scale) (b) Mesh near the bond area

Figure 7 Boundary conditions and Zoomed-In Mesh view.

Two material models were used in the study; a simple linear elastic model for titanium, and a linear elastic–plastic for polyimide. The linear-elastic model is an ABAQUS standard material model, which requires two properties: the modulus of elasticity and Poisson's ratio. The values of 120.0 GPa and 0.32, respectively, were used for titanium. The second model is also available in ABAQUS, which uses the classic von Mises yield criterion. The model requires modulus of elasticity, Poisson's ratio, and stress-strain data in the plastic region. The modulus of elasticity and Poisson's ratio for polyimide were taken to be 5.2 GPa and 0.34, respectively. The stress-strain response of polyimide is given in Table I that was used to input the plastic portion of the curve. The material property data was obtained from www.matweb.com. Due to the large deformation of polyimide under tension, the stiffness matrix has to be updated at each incremental applied load. This is achieved by turning on the geometric nonlinearily option using a standard ABAQUS keyword (e.g. *loadstep, nlgeom).

TABLE I Stress-strain data for polyimide used in FEA

Stress (MPa)	0	69	145	195	225	270	300	310
Strain	0	.0133	0.1	0.2	0.3	0.5	0.7	0.85

TABLE II Failure loads for titanium/polyimide samples

Bimaterial system	Average bond strength (N/mm)	Std. Dev. (N/mm)	Laser power (W) and Laser head speed (mm/min)
Titanium /polyimide— TYPE 1 (10*)	3.47	0.99	2.2 W, 100 mm/min
Titanium /polyimide— TYPE 2 (5*)	2.51	0.72	3.8 W, 1300 mm/min

*Number of samples tested

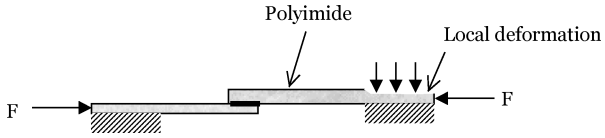

Figure 8 Local deformation of polyimide at the grip.

5. Results

5.1. Experimental

It is mentioned earlier that all of the samples were tested for bond strength using a microtester. However, there is a challenge to grip flexible materials or structures to obtain their mechanical behavior. For example, when polyimide side of the sample is mounted in the microtester, a large preloaded compression force can be introduced to the specimen due to the deformation of the polyimide caused by the compression force of the clamps (Fig. 8).

By monitoring all 6-axis forces and moments, and releasing any unnecessary mounting forces by micropositioning the corresponding stages during or after mounting the sample, those undesirable forces/moments were reduced to zero. The failure loads obtained for all samples were divided by the corresponding bond lengths to calculate the failure load per unit bond length. The bond lengths were measured using an optical microscope prior to testing the samples. Test results for both types of the samples prepared with different laser parameters are presented in Table II. It is observed that the average failure strength of type 2 samples is 2.51 N/mm, and is well below the failure strength of the type1 titanium samples (3.47 N/mm). Because the bonds for the type 2 samples were prepared using very high scanning speed, the laser had less time to interact with the titanium surface that may have resulted in poor chemical bonds between titanium and polyimide. It is thus clear that the laser power and scanning (feed) speed play an important role in attaining highest possible failure strength. A comprehensive study is underway to find the optimum laser power and scanning speed that can generate maximum bond strength for the titanium-polyimide material system.

The failed samples were analyzed by capturing images of the failure surfaces using an optical microscope. Figs. 9 and 10 show representative images of type 1 and type 2 titanium samples, respectively. The bond width was measured to be between 200 and 300 μm, although the size of the laser spot was 800 μm. This is probably due to the Gaussian power profile of the laser beam that was used in the bonding process: only the part of the laser beam cross-section with power above a certain threshold could generate good (chemical) bonding. It is also clear from the images that bond width for the type 1 samples are larger than the type 2 samples. The amount of polyimide traces on the failed titanium surface of type 1 samples (see Fig. 9) is also higher than that on the failed titanium surface of type 2 samples (see Fig. 10). From the micrographs of polyimide surfaces as well from the clear titanium surface, it is apparent that the type 2 samples failed predominantly at the interface due to shear. The laser power with high feed speed has possibly generated low interface strength which resulted in shear type failure. In contrast, the wide polyimide traces on the failed titanium surface along with the absence of smooth failed surface in the polyimide portion indicates that the failure mechanism was dominated by adherand failure for type 1 samples. This again confirms that the type 1 system offers higher adhesion than the type 2 does, which resulted in higher bond strength for titanium samples.

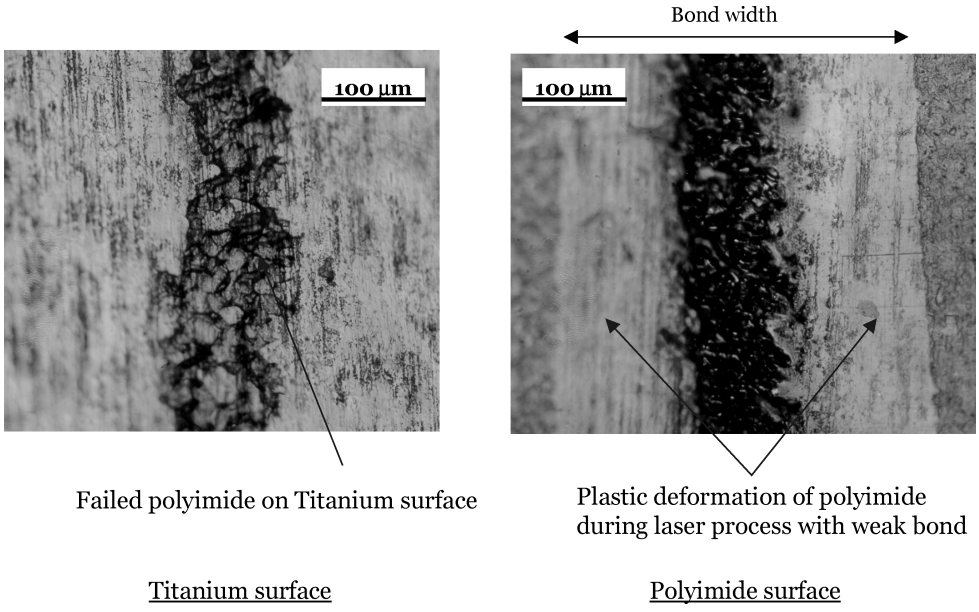

Figure 9 Microscopic pictures of a failed titanium-polyimide (Type 1) sample.

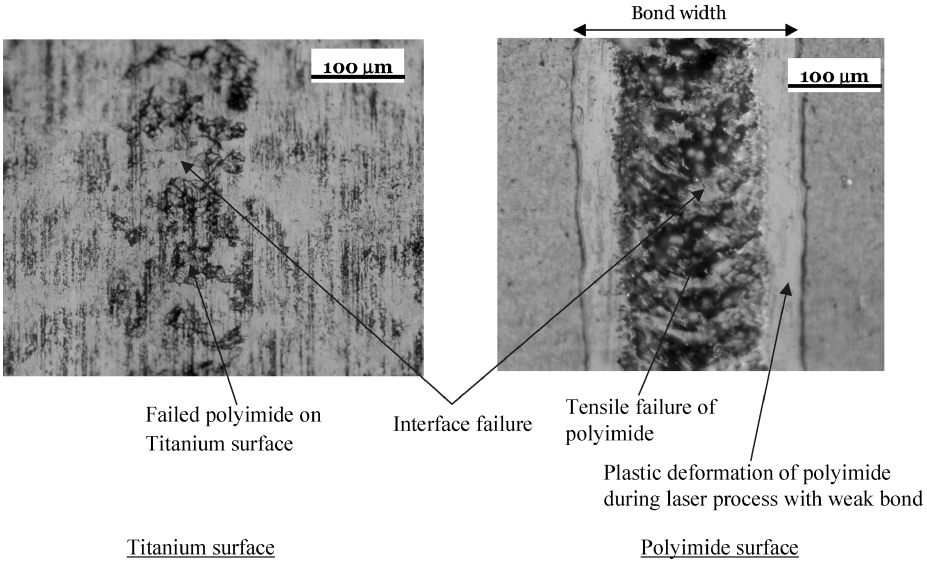

Figure 10 Microscopic pictures of a failed titanium-polyimide (Type 2) sample.

The XPS measurements showed that the breaking of the joint occurred in the polyimide plate. No Ti was detected on the polyimide side of the interface, whereas the spectra taken from the Ti side clearly showed the presence of nitrogen. The only source of nitrogen can be polyimide residue (i.e. the very polyimide material forming the laser joint with Ti) on the Ti plate. In addition high-resolution XPS spectra of the carbon 1s line, shown in Fig. 10(A), revealed the existence carbon configurations characteristic of polyimide and not expected otherwise (e.g. carbonyl groups, ─C═O). XPS Ti2p-line depth profile measurements (Fig. 11(B)) suggested the formation of new oxide, carbide, and mixed (thick arrow in Fig. 11(A)) Ti atom bonding configurations at the interface. These XPS results gave clear evidence for the formation of a sharp (with thickness in the order of 10nm) and strong interface based on titanium-oxygen and titanium-carbon chemical bonds. Full details of this XPS study are presented in reference [22].

5.2. Finite element analysis

Load-displacement response of the titanium-polyimide sample obtained from the finite element analysis (FEA) is presented in Fig. 12. As the model was developed considering strong interface between titanium and polyimide, the load displacement response has been compared with the experimental results for the type 1 samples. Because, it is already confirmed through the microscopic analysis that the type 1 system does have high bond strength. From the figure, it is apparent that the FEA prediction matches reasonably well with the experimental data, considering the slight offset in the experimental load-displacement plots.

Variation in the shear and von Mises stresses along the width of the bond at the titanium-polyimide bondline are depicted in Figs. 13 and 14, respectively. The results presented in those figures are collected from the nodal points at the interface at the end of 0.43, 0.52, 0.60, 0.69, and 0.82 mm displacement loads. The shear stress profile is observed to be similar to that found

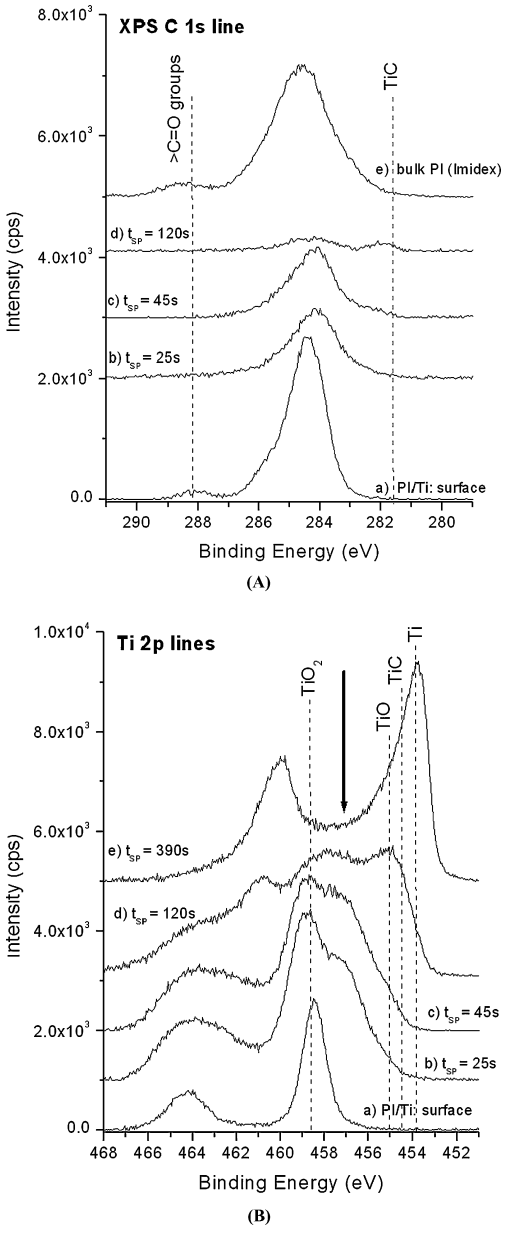

Figure 11 XPS spectra taken from the Ti side of the peeled off sample. (A) C1s line and (B) Ti2p lines spectra taken after the specified spurting times (t_{SP}).

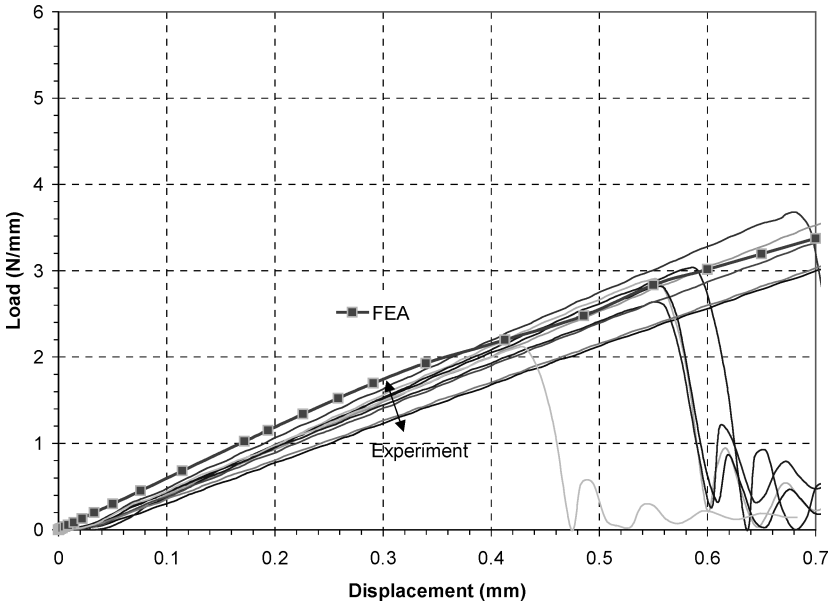

Figure 12 Experimental load-displacement plots for titanium (Type 1) samples along with corresponding finite element data.

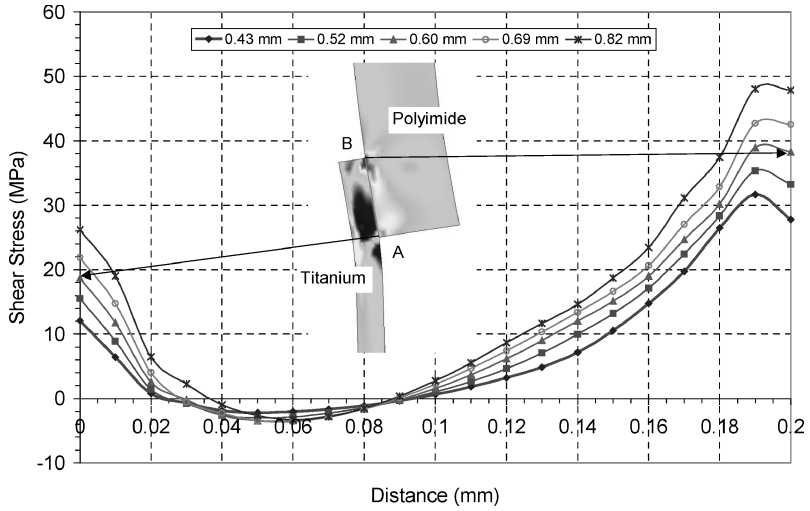

Figure 13 Shear stress variation at the Titanium-polyimide interface along the bond-width (FEA results at 0.43–0.82 mm displacement loads).

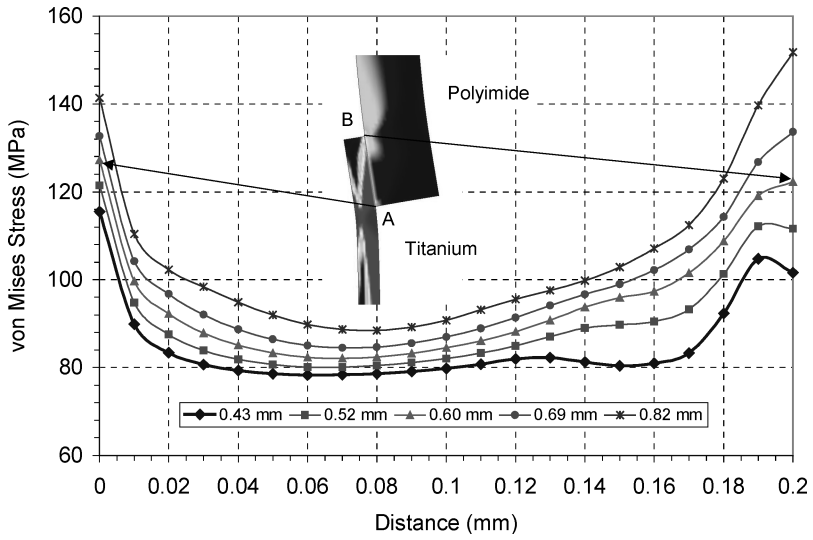

Figure 14 von Mises stress variation at the Titanium-polyimide interface along the bond-width (FEA results at 0.6 mm displacement load).

in adhesively bonded lap shear samples under tension [21]. It is apparent from Fig. 13 that shear stress increases with applied load which is obvious, however, the stress is zero at about 0.9 mm from point A on the bondline for all load steps. This is due to the reason that the substrates in the bond zone rotated about the z point. It is observed that high shear stresses attained at the edges A and B, while it remains maximum at B. Maximum shear stress at 0.82 mm displacement is observed to be 48 MPa, which is well below the shear strength of both polyimide and titanium. From Fig. 14, it is clear that von Mises stress is also high at the end locations A and B, and is minimum somewhere between A and B on the bondline. The location of maximum von Mises stress shifts from point A to point B at 0.6 mm displacement load. The maximum von Mises stress at 0.6 mm load is 127 MPa at location A, which is close to the failure strength of polyimide. Please note that the failure strength of bulk polyimide material is 130 MPa, and is assumed to be same for 180 μm thin polyimide film. Since the maximum stress is still below the shear strength of polyimide and since the von Mises stress is close to failure strength of polyimide at 0.6 mm load, the type 1 samples are predicted to fail at 0.6 mm displacement load due to the tensile type of polyimide substrate. The tensile failure of polyimide is attributed to the rotation of the substrates near the bond area. It is also observed from the experimental results as shown in Fig. 12 that few of the samples did fail at 0.6 mm load.

The contour plots of in-plane shear and von Mises stresses at 0.6 mm load are depicted in Figs. 15 and 16, respectively. Deformed shape in the figures represents the actual relative deformation with no displacement scaling up. From both the figures, it is apparent that the substrates have rotated substantially although the system was loaded with tension in y-direction. This

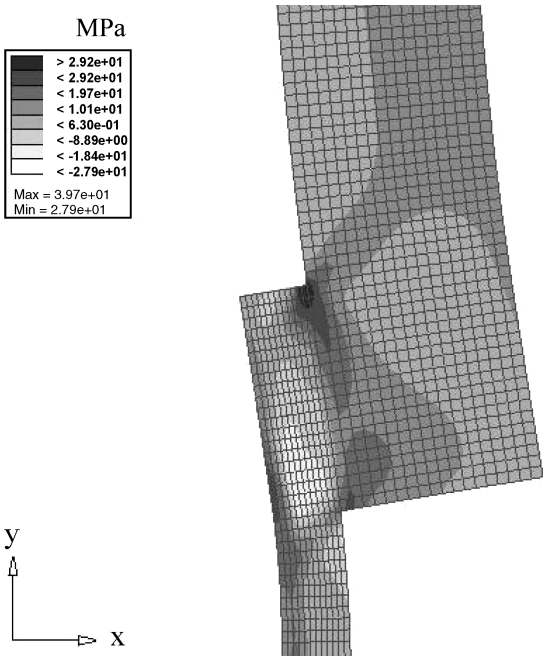

Figure 15 Contour of in-plane shear stress distribution (FEA Results at 0.6 mm displacement load).

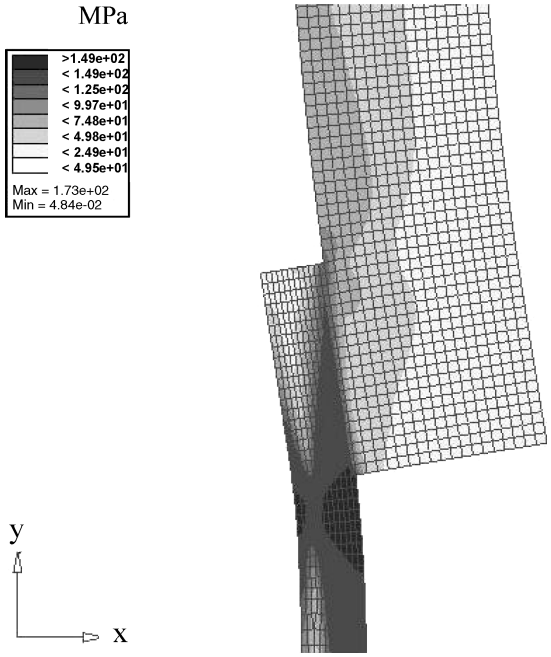

Figure 16 Contour of von Mises stress distribution (FEA Results at 0.6 mm displacement load).

phenomenon is common in bimaterial joining systems due to the high differential deformations near the joint, and the amount of rotation depends on thickness and mechanical properties of the substrate materials. This rotation results in the development of all possible stress components with high stress gradients within the bond region. The attainment of high stress magnitude at the two edges (near the locations A and B) is attributed to the singularity in geometric and mechanical properties of substrate materials. From Figs. 15 and 16, it is also observed that the stress distribution is uniform in the substrate away from the joining region. Maximum von Mises stress is observed to be developed in titanium near the point A although its magnitude did not exceed the high failure strength of titanium. Bending of the titanium substrate in the vicinity of point A resulted in bending stress that has contributed to additional increase in von Mises stress in that region.

6. Summary

Laser joined titanium-polyimide samples were tested for bond strength, and was observed that the laser bonding parameters such as laser power and feed speed affect the bond strength of all material systems. The type 1 (lower laser power with lower speed) system was observed to offer high bond strength, and the failure mechanism was predominantly tensile type failure of the polyimide substrate. This is due to the rotation of the bond during tensile load as was clear from the FEA results. Prediction of the failure load from FEA model was well in agreement with the experimental results. The effect of bond strength on the failure mechanism can also be predicted using FEA modeling scheme, and will be presented in a later study.

Acknowledgments

The authors acknowledge the financial support from Michigan Economic Development Corporation (MEDC), and Michigan Life Sciences Initiative (MLSC) to perform this study.

References

1. K. JEFFREY, "The Implantable Defibrillator and American Health Care" (2001) p. 408.
2. S. MIYOSHI, T. IFUKUBE and J. MATSUSHIMA, *Transactions of the Institute of Electrical Engineers of Japan Part A* **118-A**(3) (1998), 260.
3. U. MEYER-BAESE, A. MEYER-BAESE and H. SCHEICH, in Proceedings of SPIE—The International Society for Optical Engineering, (1997), Vol. 3077, p. 582.
4. R. G. DENNIS, D. E. DOW and J. A. FAULKNE, *Medical Engineering & Physics* **25**(3) (2003) 239.
5. B. LITT, in IEEE Proceedings of the 23rd Annual EMBS International Conference (October 25-28, Istanbul, Turkey, 2001) p. 4124.
6. J. T. SANTINI, in Proceedings of the 4th Int. Symposium on BIOMEMS, (Cambridge MA, 2002).
7. R. S. SHAWGO, A. C. R. GRAYSON, Y. LI and M. J. CIMA, *Current Opinion in Solid State and Materials Science* **6**(4) (2002) 329.
8. M. L. HANS and A. M. LOWMAN, *Current Opinion in Solid State and Materials Science* **6**(4) (2002) 319.
9. N. S. PEACHEY and A. Y. CHOW, *Journal of Rehabilitation Research and Development* **36**(4) (1999) 381.
10. A. Y. CHOW and V. Y. CHOW, *Neuroscience Letters* **225**(1) (1997) 13.
11. M. S. HUMAYUN, J. D. WEILAND, G. Y. FUJII, R. GREENBERG, R. WILLIAMSON, J. LITTLE, B. MECH, V. CIMMARUSTI, G. V. BOEMEL, G. DAGNELIE and E. D. JUAN JR, *Vision Research* **43** (2003) 2573.
12. J. MEYER, T. STIEGLITZ, O. SCHOLZ, W. HABERER and H. BEUTEL, *IEEE Transactions on Advanced Packaging* **24**(3) (2001) 366.
13. M. J. WILD, A. GILLNER and R. POPRAWE, *Sensors and Actuators A* **93** (2001) 63.
14. G. NEWAZ, A. MIAN, L. VENDRA, D. GEORGIEV, T. MAHMOOD, G. AUNER, R. WITTE and H. HERFURTH, in Proceedings of the International Congress on Materials Science and Nanotechnologies (European Academy of Science, Brussels, Belgium, October 2003).
15. V. A. KAGAN, R. G. BRAY and W. P. KUHN, *Journal of Reinforced Plastics and Composites* **21**(12) (2002) 1101.
16. V. A. KAGAN and G. P. PINHO, *Journal of Reinforced Plastics and Composites* **23**(1) (2004) 95.
17. P. A. HILTON, I. A. JONES and Y. KENNISH, in Proceedings of SPIE—The International Society for Optical Engineering (2002) Vol. 4831, p. 44.
18. I. BAUER, U. A. RUSSEK, H. HERFURTH, R. WITTE, S. HEINEMANN, G. NEWAZ, A. MIAN, D. GEORGIEV and G. AUNER, in Proceedings of SPIE—Photonics West LASE 2004: Lasers and Applications in Science and Engineering conference, (San Jose, California, 24–29 January 2004).
19. M. LU, Z. QIAN, W. REN, S. LIU and D. SHANGGUAN, *Intern. J. Solids Struct.* **36**(1) (1999) 65.
20. ABAQUS User's Manual, Version 6.2, Hibbit, Karlsson and Sorensen, USA.
21. C. YANG and S. PANG, *J. Engng Mater. Techn.* **118** (1996) 247.
22. D. G. GEORGIEV, R. J. BAIRD, G. NEWAZ, G. AUNER, R. WITTE and H. HERFURTH, *Applied Surface Science* **236**(1) (2004) 71.

Received 26 January
and accepted 20 July 2004